3D Printed Drone
Drone C
Spring 2024
Final Report

By

DESCENDER Inc.

Hoa Nguyen
Peter Nguyen
Yugesh Shrestha
Phat Nguyen
Cavin Van

Prepared for
Dr. Woods
Dr. Allsup
Dr. Taylor

May 3, 2024

Abstract

UTA has held the 3D-Printed Aircraft Competition (PAC) for eight years. A rotatory drone was 3D printed through additive manufacturing to compete in the 3D-printed aircraft competition. The drone was developed in several parts, including electronics, drone frame, arms, and drag device. Each component was designed and researched to be lightweight with minimal vibration and stiff structure. The electronics were chosen to ensure enough thrusting force and power to withstand the weight of the drone and drag device. The 3D filament chosen for the drone is abs, which was chosen based on its performance to heat, low density, and high elastic modulus, ensuring a stiff structure. Using topology optimization and solid works a 5” arm was created with stiffness and weight as our main objective. The drag device was created as a hinge, so the flaps were able to descend slowly, our main goal was to increase surface area without any electronic actuation. The design was further improved and tested through simulation and experimentation to ensure maximum stiffness, minimum frequencies, fast response and stable flight. The progression from the start to the final design took many iterations, but each iteration improved the overall design. The final iteration of our design was able to achieve 30 feet in the 8 second time frame and a free fall time of 3 seconds.

Personnel

Hoa Nguyen
Lead Engineer
hoa.nguyen6@mavs.uta.edu

Peter Nguyen
Analysis Engineer
petertung.nguyen@mavs.uta.edu

Yugesh Shrestha
Design Engineer
yugesh.shrestha@mavs.uta.edu

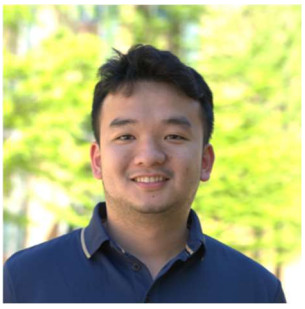

Phat Nguyen
System Engineer
phat.nguyen4@mavs.uta.edu

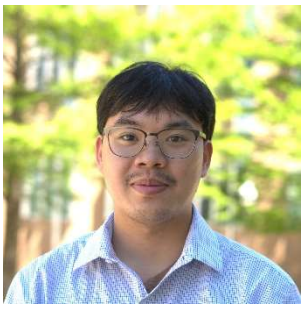

Cavin Van –
Manufacturing Engineer–
cavin.van@mavs.uta.edu

Faculty Advisors

Dr. Taylor
taylorrm@uta.edu

Dr. Allsup
thomas.allsup@uta.edu

Table of Contents

Nomenclature

a - Acceleration [m/s^2]
A - Surface Area [m^2]
C - Coefficient [-]
D - Drag Force [N]
F - Force [N]
g - Gravity [m/s^2]
H - Height [m]
L - Length of Arm [mm]
m - Mass [kg]
M - Moment [N*mm]
ρ - Density [kg/m^3]
P - Power [W]
R - Reaction Force [N]
t - Time [s]
T - Torque [N*mm]
v - Velocity [m/s]
V - Shear [N]
ω - Angular Velocity [rad/s]
x - Location [mm]

Subscript

d - Drag
f - Final
i - Initial
t - Terminal
total - Total

1. Introduction

With the recent technological advancement of additive manufacturing, it has been widely popular in today's manufacturing process. One form of additive manufacturing is called fused deposition modeling (FDM) 3D printing. With the advancement of FDM 3D Printing, it is widely used for rapid prototyping due to its consistency, reliability, and fast printing. Not only can FDM 3D printing be used for rapid prototyping, but it can also be another manufacturing method to produce parts for a product. With that, this project aims to use FDM 3D printing for rapid prototyping and producing a drone model that is completely 3D printed and functional.

2. Motivation

This is the 8th annual 3D-Printed Aircraft Competition (PAC) that UTA has hosted. Where students will compete to develop a 3D-printed aircraft using additive manufacturing. Currently, there are two aircraft categories: fixed and rotary wing. For the rotary wing category, students will create an aircraft where lift is generated by the propelling motion of the motors. Students will also compete in design and overall flight time when only 8 seconds of power is given to fly 30 feet. This means the team with the longest overall flight time, ascending and descending the aircraft, will win the competition.

Figure 1 Competition Poster

The goal is to create the final drone product to compete in the rotary aircraft category and fly off on July 13, 2024. The project aims to win the longest flight duration using the 3D-printed drag device and drone.

3. Theory

3.1. Drone Arm

The drone arm can be seen as a cantilever beam supported by the frame. When a propeller is added to a motor, the lift load is applied to the arms' ends. Figure [x] displays the arm's free-body diagram.

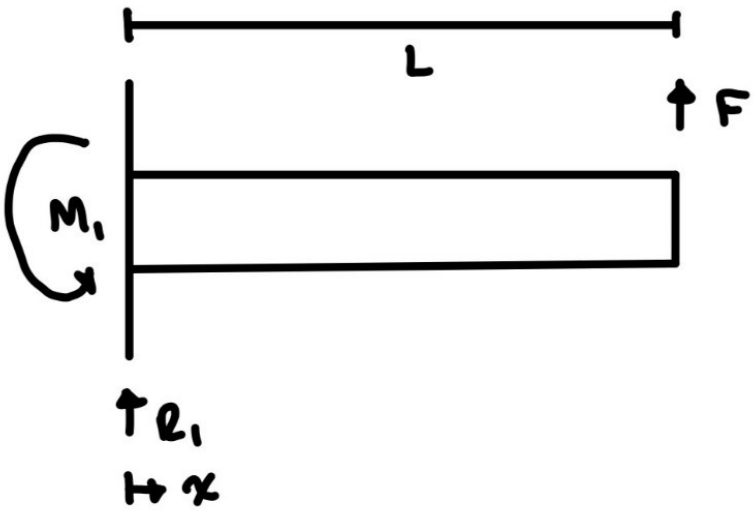

Figure 2 Free-Body Diagram of Drone Arm

To calculate the reaction forces, use the principle of equilibrium and have the sum of forces equal zero. The resultant forces can be found below.

$$R_1 = F$$

$$M_1 = F * L$$

With the help of singularity equations, shear and moment can be found in the equation below.

$$V = M_1 < x >^{-1} + R_1 - F < x - L >^0$$

$$M = -M_1 + R_1 x - F < x - L >^1$$

With the full analysis of this equation, the max shear will occur throughout the whole arm. The max moment will occur at the resultant forces; this is useful to determine the length of the arm to minimize this moment.

3.2. Drag Device

The design of the drag device was based on increasing the surface area to increase the drag force experienced by the device, which would lead to an increase in descent time. Descent time was calculated first by determining the terminal velocity that the device was traveling before hitting the ground. The formula used to calculate the terminal velocity of the device is shown below.

$$v_t = \sqrt{\frac{2W}{C_d \rho A}}$$

Where V_t is the terminal velocity of the device once it enters free fall, ρ is the density of the air, A is the surface area of the drag device, and W is the weight, C_d is the drag coefficient of the drag device.

Initially, the flat plate's drag coefficient was used to calculate the terminal velocity. Weight was calculated by determining the material's volume and density. The gravity and density of the air at 90 degrees Fahrenheit at a Latitude of 32.73, a longitude of -97.11, and an elevation of 189.89 above sea level were used.

Time of descent was calculated in two phases; 1st phase was when it took the device to get to terminal velocity from the free fall, and 2nd phase was when it took the device to hit the ground after reaching terminal velocity. The formula used for this calculation is as follows:

1st phase:

$$t_1 = \frac{v_f - v_i}{g}$$

where the initial velocity is zero, the final velocity is the terminal velocity, and g is the acceleration due to gravity. The distance traveled to reach terminal velocity was also calculated using the following formula shown below:

$$H_1 = \frac{v_f^2 - v_i^2}{2g}$$

2nd phase:
Given that the drone is estimated to drop from a height of 9.14m (30ft), the time it took to reach the ground after reaching terminal velocity was calculated using the following formula.

$$t_2 = \frac{9.14 - H_1}{v_t}$$

The total time of descent was calculated by adding those two times together.

$$t_{total} = t_1 + t_2$$

4. Design

4.1. Drone Specification

Protecting the electronic components in the drone body was ideal. A modular design, where the arms can be replaced, would have been ideal if the arms had been destroyed in the flight tests. A lower center of gravity is crucial to the design as it helps the overall stability of the device. A stiff structure reduces vibrations in the system, or instability can occur.

4.2. Drag Device Specification

The drag device was designed by keeping the weight of the device and the drone's main body in mind. The goal was to stay under 600 g for the entire assembly. Weight reduction was also achieved by having the drag device deploy with the help of air resistance instead of servos.

4.3. Electronic Specification

- Flysky remote control and receiver.

This allows the remote controller to communicate with the drone and receive any controls.

- 4 Cells LiPo battery; 650mAh, 90C, 15.8V

A 650mAh (0.65Ah) battery with a 90C discharge rate can provide 90 times its capacity. So, 90 x 0.65Ah = 58.5A, which means the battery can safely provide 58.5A amps of current for 30 seconds.

- Xing 2208 1800kv motors

2208 => stator's diameter = 22mm and height = 8mm, 1800kv=> 1800 rpm per volt of the power supply. KV rating indicates the motor's RPM per volt. At 22.2V, the motor's theoretical maximum RPM is 1800 * 14.8 = 26640 RPM.

- Nazgul F5 – Tri Blade Propeller – 5.0x3.5x3
  5-inch diameter = 0.127, 3.5-inch pitch

- SpeedyBee F405 V4 BLS 55A 30x30 FC&ESC Stack

Verification:

Required force:

$$F = ma$$

$$F = (0.6\ kg)\left(10.5415\frac{m}{s^2}\right) = F_{required} = 6.325\ N => 1.58\ N\ each\ motor$$

$$H = v_i t + \frac{1}{2}at^2 \quad (goal: climb\ up\ to\ 30ft\ in\ 5s)$$

$$30ft = 9.144m = 0 + \frac{1}{2}a(5)^2 => a = \frac{2 * 9.144}{25} = 0.7315 => a_y = 0.7315 + 9.81 = 10.5415\frac{m}{s^2}$$

Motors:

$$1800kv * 14.8V = 26640\ RPM = 2789.7\ rad/s \quad (\omega)$$

Propeller:

$$v_i = \frac{v_{inf} + v_s}{2}$$

$$v_s = 2v_i\ (since\ v_{inf} = 0)$$

$$F = \dot{m} * (v_s - v_{inf})$$

$$\dot{m} = \rho A v_i => F = \rho A v_i (2v_i - 0) = 2\rho A v_i^2$$

$$P = F * v_i = 2\rho A v_i^2 v_i = 2\rho A v_i^3$$

$$=> T = (2\rho A P^2)^{\frac{1}{3}} * \eta_{propeller} = \left(2\rho\pi\left(\frac{D}{2}\right)^2 P^2\right)^{\frac{1}{3}} * \eta_{propeller}$$

$$P = v * i = 14.8\ V * 0.65\ A * 3[C] = 28.86\ W$$

$$assump\ \eta_{battery} = 60\% => P = 17.3W$$

$$assump\ \eta_{propeller} = 0.8 => F = \left(2 * 1.225 * \pi\left(\frac{0.127}{2}\right)^2 17.3^2\right)^{\frac{1}{3}} * 0.8 = 1.68\ N$$

$$with\ 4\ motors$$

$$=> the\ total\ thrust = 1.68 * 4 = 6.72\ N$$

$$=> total\ discharge\ rate = 12$$

$$=> Battery\ time : 225s$$

So, with the chosen components, the motor can produce sufficient power to achieve the goal with a discharge rate of 12. The thrust calculation was computed with a blade efficiency of 80%. Blade-Element Theory (BET) and Vortex theory must be considered for more accurate thrust predictions. The theoretical battery time is calculated to be 225 seconds, equivalent to 3.75 minutes, sufficient for three flights in competition.

Torque (τ) calculation:

$$Power\ (P) = \frac{\tau}{\omega} => \tau = P\omega = 16W * 4185.5\frac{rad}{s} = 66968\ N * m = 66.96N * mm$$

4.4. Material Selection

The materials investigated for this project were TPU, PLA, PETG, and ABS. The main criteria for choosing a material were based on a high heat resistance material, high elastic modulus, and low density.

Table 1 Material Properties

Materials	Heat Resistance Temperature (°C)	Elastic Modulus (MPa)	Density (g/cm^3)
TPU	N/A	N/A	1.22
ABS	87	1880	1.05
PLA	57	2750	1.24
PTEG	69	1670	1.25

A highly heat-resistant material would be more resistant to softening as temperature increases. Materials with low heat resistance would likely soften and deform in the summer. For instance, PLA is affected by UV light weathering, which reduces the material's softening temperature, so using PLA for the final device is not advised. However, because PLA is very easy to use when 3D printing, it is ideal for prototyping compared to the other materials.

Investigating the material's elastic modulus can achieve high stiffness, resulting in the arms having a very small deflection when loads are applied. The best materials would be ABS and PLA because they would allow for higher stiffness in the arms, whereas TPU is very elastic and works best as a damper.

A material with the lowest density would allow the drone to be lightweight, increasing the time of our descent. ABS was chosen because it has the highest heat resistance temperature, the lowest density, and the second-highest elastic modulus.

4.5. Arm Design 1

The first design is displayed in Figure 3. This model ultimately did not work, as the arms were too long and caused the structure to break at the root of the arms. With that, it was too heavy and was weak when it came to torsional. A vibration test was run to determine if the system would experience any vibrations. The results from the vibration test showed that there were vibrations in the system, which would cause instability. So, a redesign of the arms will be considered to combat the vibration issues.

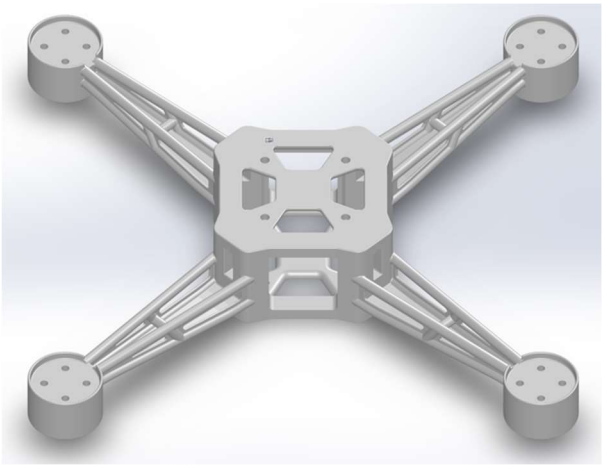

Figure 3 1st Iteration Arm

4.6. Arm Design 2

From the first design, where there were issues at the root, the drone arm length was shortened to reduce the moment at the root. The design goal of the arms is to keep them stiff and lightweight. With the help of topology optimization, the drone arm was designed and shown in Figure 4. The second iteration is designed to be stiff to combat the forces of lift and torsional at the end. Overall, this is a better design than the previous iteration due to its reduced moment at the root, stiffness, and lightweight. This structure will also help reduce vibrations experienced in the first iteration.

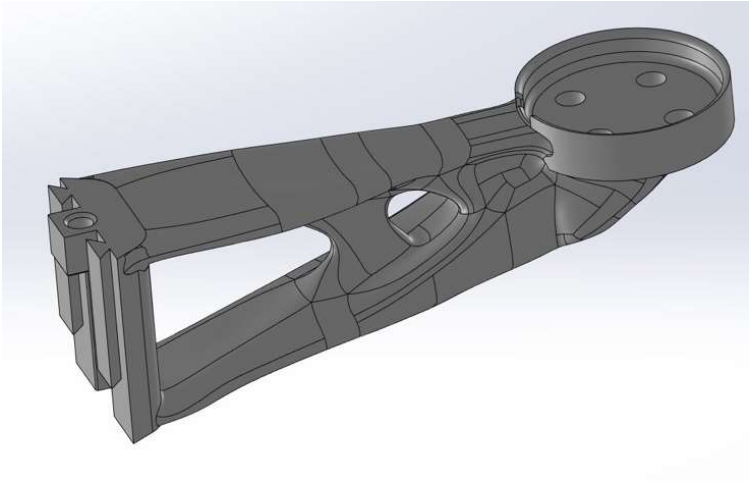

Figure 4 2nd Iteration Arm

4.7. Drag Device Design 1

The initial prototype of the drag device was created based on a modular design. The circular flaps at the end of the arms were to generate drag force. The arms could rotate vertically about the point of contact at the base. This design choice was made so that the drag device would deploy with the help of air resistance. During numerous tests of this prototype, it was observed that the circular flaps did not generate enough drag for the drag device to slow down. Still, the arm's ability to rotate vertically during deployment made the descent stable possible.

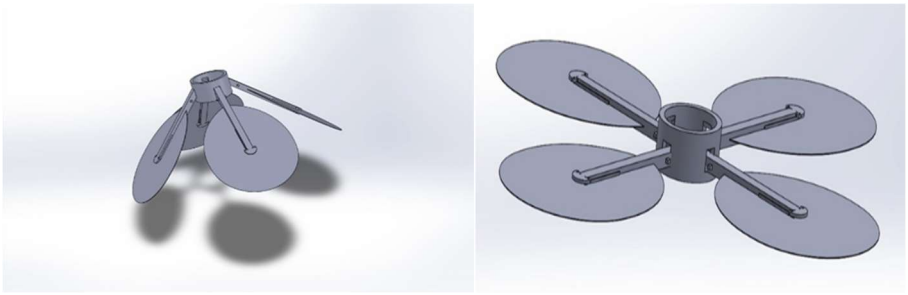

Figure 5 1st Concept of Drag Device

4.8. Drag Device Design 2

The second prototype was designed to direct the airflow underneath the drag device. The motivation for designing this prototype was taken from the sugar glider's gliding motion during free fall. The curved wing design was incorporated to direct the airflow outwards from the center cross-section to achieve drag. While testing this prototype, the amount of surface area of the device helped generate enough drag force to slow down the device, but it was observed that the device had unstable descent on multiple test runs. The inability of the air to pass through the center created turbulence, which was the main reason for the unstable descent. Fixed wings also meant the rotors could not direct air to the ground to generate enough lift for the drone to fly.

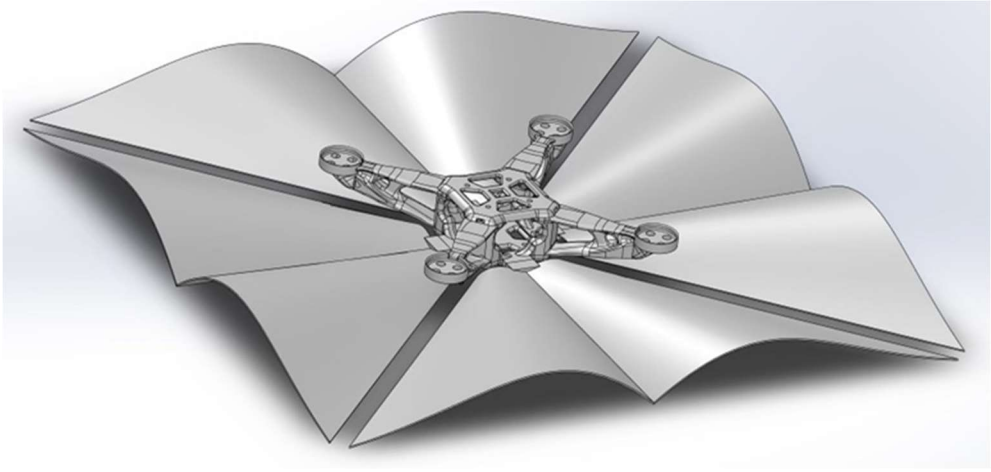

Figure 6 2nd Concept of Drag Device

4.9. Drag Device Final Design

The final design of the drag device was a collaboration of two previously designed prototype ideas. The flaps from the 2nd prototype were incorporated to deploy only due to air resistance. The hinge-like design between the flaps and the drag arm helped the flaps to rotate about the point of contact. Constraints for how much rotation the flaps can make were created by introducing stoppers on the arms, which also dictated the flaps' deflection. Positioning radially outward flaps helped create space at the center of the device, which would be crucial in directing airflow through the center. Pillar structures were assimilated between the drone and drag arms to support and stabilize the structure.

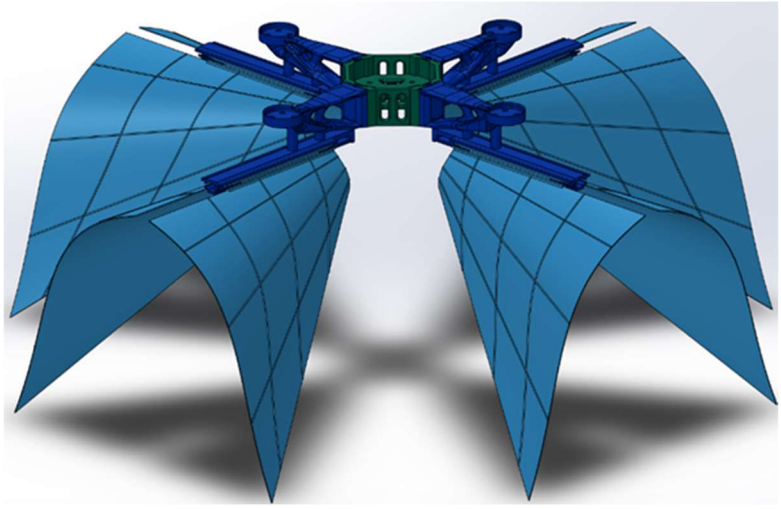

Figure 7 Current Design

5. Analysis

5.1. Drone Arm 2

The quadcopter drone's structural integrity and performance were evaluated using finite element analysis on ANSYS. For structural analysis, the purpose was to examine the drone's behavior under different loading conditions, including its weight and aerodynamic forces, such as the thrust force. The drone's weight acts as a downward force at the center mass of the drone. The thrust force from each propeller generates lift and acts as an upward force. Each arm was modeled as a cantilever beam, fixed at one end and free at the other. There were fixed supports placed at the screw holes of each arm, where it was connected to the base of the drone. The lifting force and weight were also accounted for.

The structural analysis results calculated the total deformation, Von Mises stresses, and safety factor. The results of total deformation showed a uniform deformation, where a maximum total deformation of 0.063 mm occurred at the propellers and decreased uniformly towards the screw holes to a minimum total deformation of 0 mm. It signifies that the drone had a high stiffness. A safety factor of 15 indicates that the drone was overdesigned, with unexpected loads. Although these were the results for the safety factor in ANSYS, the safety factor for the actual drone decreased due to the infill percentage, assuming solid infill when 3D printing the drone.

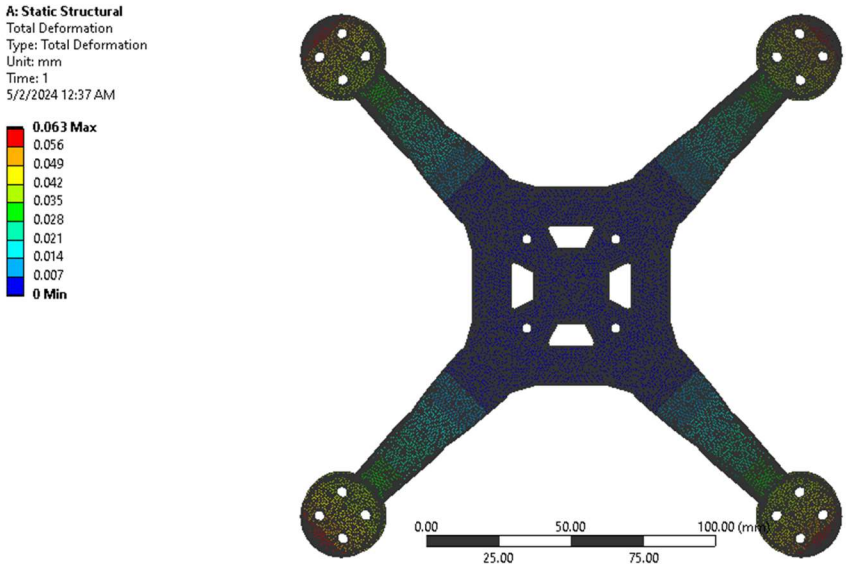

Figure 8 Total Deformation for Static Structural

Using Modal analysis in ANSYS, the drone's dynamic structure was identified by the mode shapes and their natural frequencies at different dynamic loadings or sinusoidal inputs of varying frequencies. This is where the structure experienced high-level vibrations and critical areas to add stiffeners to the part.

The analysis's results showed that the critical areas were at the ends of the arms, where it acted like a fixed free cantilever beam with loading applied at the free end. It showed that it is more likely to deflect at the tip at different dynamic loadings. The results showed that at the lowest frequency of 451 Hz, it would most likely resonate and vibrate, ultimately leading to stability and part failure when flying the aircraft. For the drone with the propellers and motors, it never reached 451 Hz, so the drone did not cause vibrations.

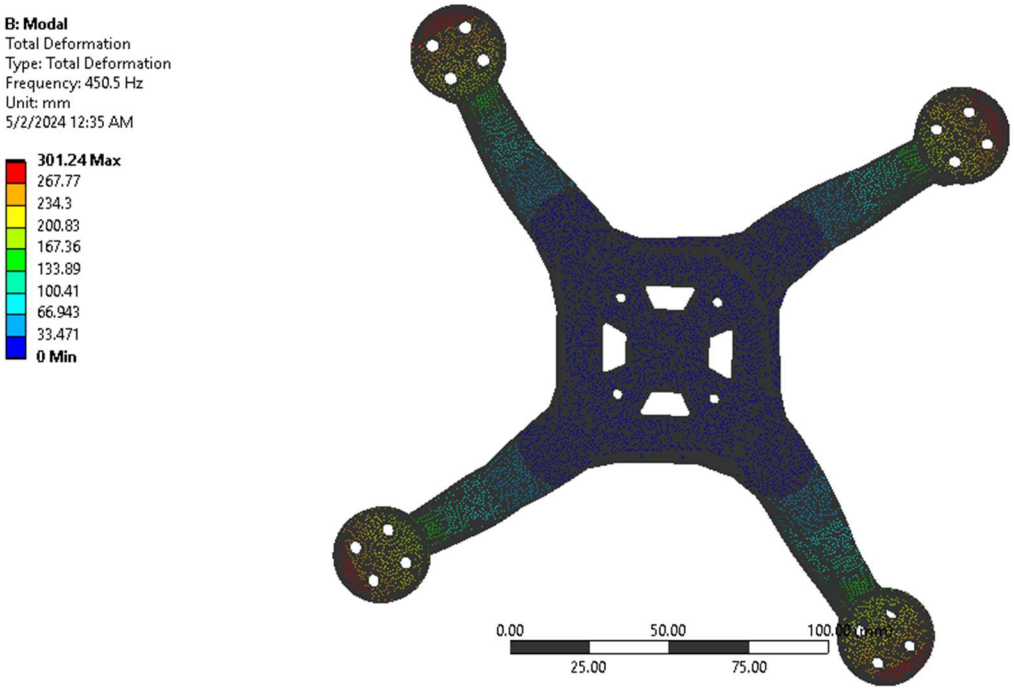

Figure 9 Total Deformation for Modal

5.2. Drag Device

Computational fluid dynamics simulation was conducted in SolidWorks using flow simulation. During the simulation, a metric unit system was chosen, and an external analysis was conducted with gravity turned on in the negative Y direction. The fluid for the simulation was air, and the terminal velocity of the device and its direction were entered. The type of flow was assumed to be laminar for this experiment. An Automatic Computational domain was created to conduct the Drag experiment. The global goal was created to track normal force in the Y direction, and the equation was entered to obtain the drag coefficient. The equation used to calculate the drag coefficient is shown below:

$$C_d = \frac{2D}{V_t{}^2 \rho A}$$

Where, C_d is the drag coefficient, D is the drag force, V_t is terminal velocity, ρ is the density of the air, and A is the device's surface area.

Quality Mesh is created to obtain adequate results for the calculations. Refinements were placed in a region surrounding the flaps because they are essential to the device's function. Once the simulation started, plots were created, and the program continued running the simulation until the goal values, i.e., the Drag coefficient in this case, converged. A graph of converging values is shown in the figure below:

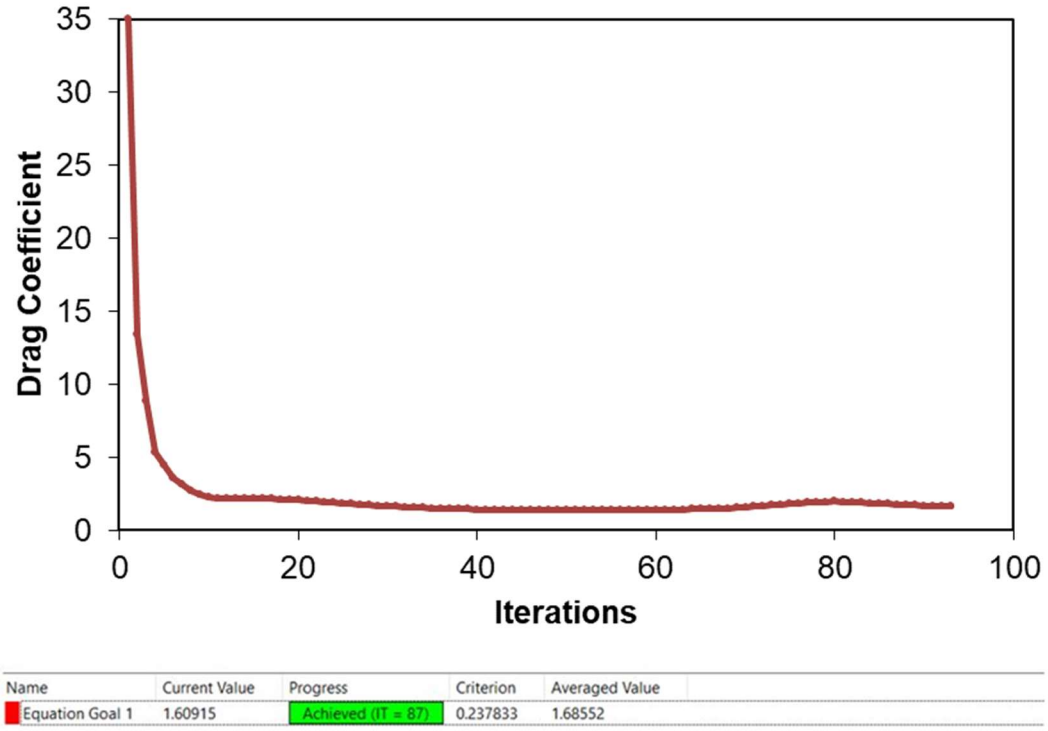

Figure 10 CFD Analysis Results

From 87 iterations, the average value of the drag coefficient was 1.69.

Cutting plots on the results helped to select the plane and parameter we wanted to inspect, which were shown in color contours depending on the values. Velocity distribution around the drag device is shown in the figure below:

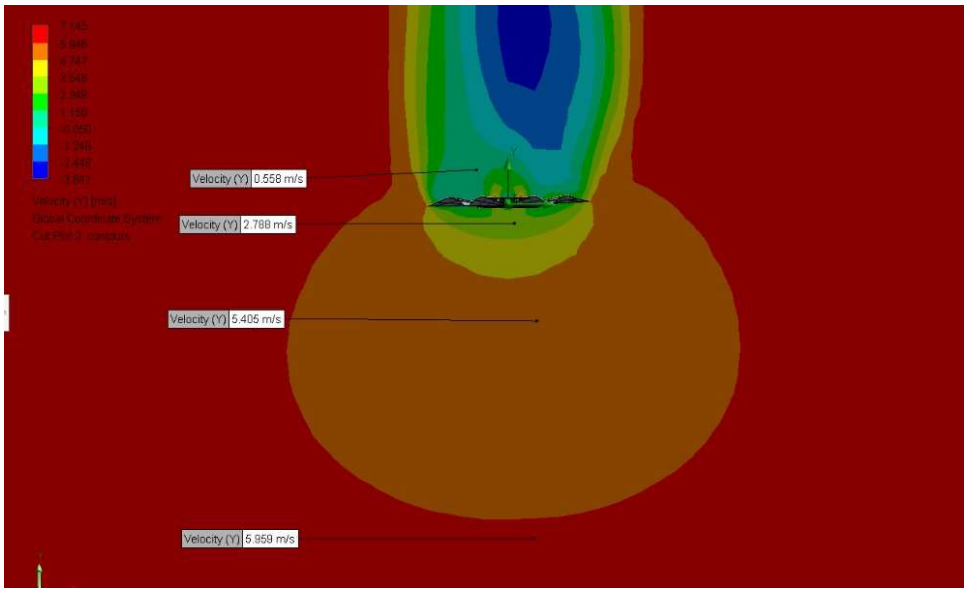

Figure 11 CFD Analysis

The drag coefficient obtained from the flow simulation was used to calculate the drag device's descent time. The table below shows the descent time of the drag device with an increase in surface area.

Table 2 Time of Descend Calculation Based on Surface Area

Length (m)	Area (m^2)	V_t (m/s)	Drag force (N)	Time to reach V_t (s)	Distance to reach V_t (m)	Time to landing (s)	Distance to landing (m)	Total time for descent (s)
0.3	0.09	6.58	3.79	0.67	2.21	1.05	6.93	1.73
0.4	0.16	5.21	4.22	0.53	1.39	1.49	7.76	2.02
0.5	0.25	4.44	4.77	0.45	1.00	1.84	8.14	2.29
0.6	0.36	3.95	5.45	0.40	0.80	2.11	8.35	2.52
0.7	0.49	3.63	6.26	0.37	0.67	2.34	8.47	2.71
0.8	0.64	3.40	7.18	0.35	0.59	2.52	8.55	2.86
0.9	0.81	3.23	8.23	0.33	0.53	2.66	8.61	2.99
1	1	3.11	9.40	0.32	0.49	2.78	8.65	3.10

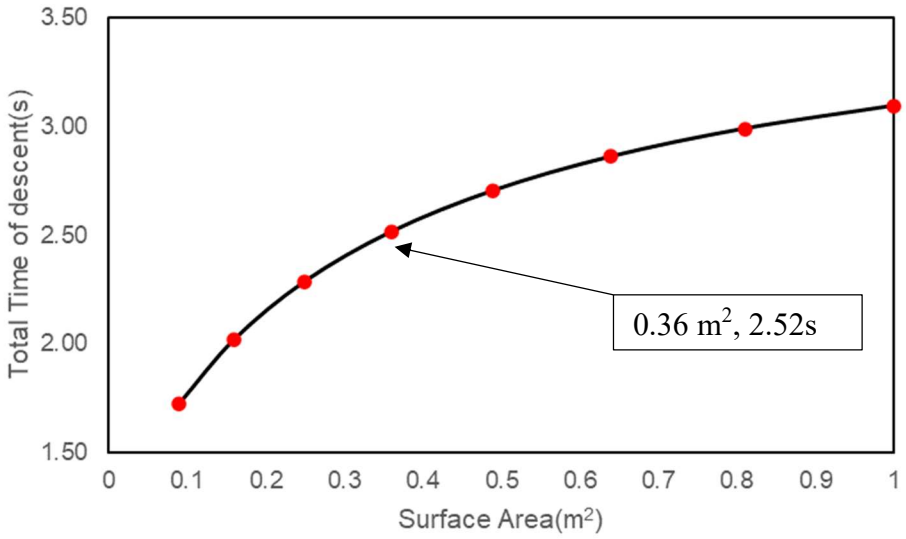

Figure 12 Time of Descend Calculation Based on Surface Area

6. Testing

6.1. Vibration Testing

During this test, the propellers will be removed from the drone, and the motors will be powered from 100 % and decreased to 40%. The structure will then be placed on a firm flat surface. During this test, it is important to observe any vibrations that the structure may encounter when the motors are at a constant 40% power. For the 1st iteration of the arms, it was found that there were vibrations present in the test. This led to the redesign of the arms, which led to the 2nd iteration. With the repetition of this test, the 2nd iteration arm did not encounter any vibrations.

6.2. Flight Testing

The drone could fly upward and downward without many stability issues during its launch. This means sufficient power is supplied to the motors, and the drone's weight is adequate for takeoff. It also has a faster response time and minimizes overshooting and system instability. There were also no implications with the drag device and drone when ascending upward because the drag device did not open until free fall.

Figure 13 Flight Test

6.3. Drop Test

During the drone's descent and its drag device counterpart, the free fall time was 3 seconds. This fall time exceeded the calculated time of 2.52 seconds based on the 600 mm flaps. During the drag device's descent, the flaps worked just as anticipated, actuating like a hinge mechanism. During the drone’s descent, the flaps are met with air resistance, which opens the flaps, creating a drag force that slows the drone’s fall.

Figure 14 Drop Test

6.4. PID Tunning

Betaflight is utilized for Drone PID tuning, with adjustments made using the following sliders:

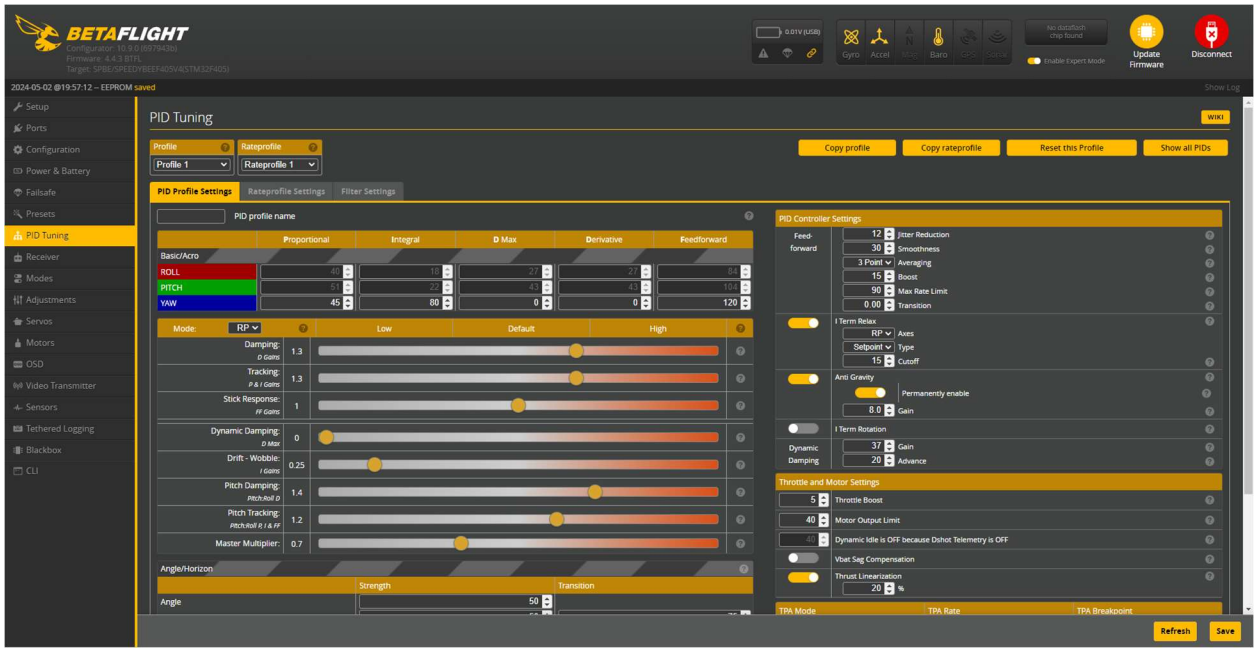

Figure 15 Betaflight Software

The tuning process begins by setting the initial tracking P&I slider value at 0.5, which is then incremented by 0.1 for each iteration. Flight tests are conducted for every increment to collect data into the drone's Blackbox for dynamic response analysis in MATLAB. The responses are recorded for P &I slider values ranging from 0.5 to 1.3.

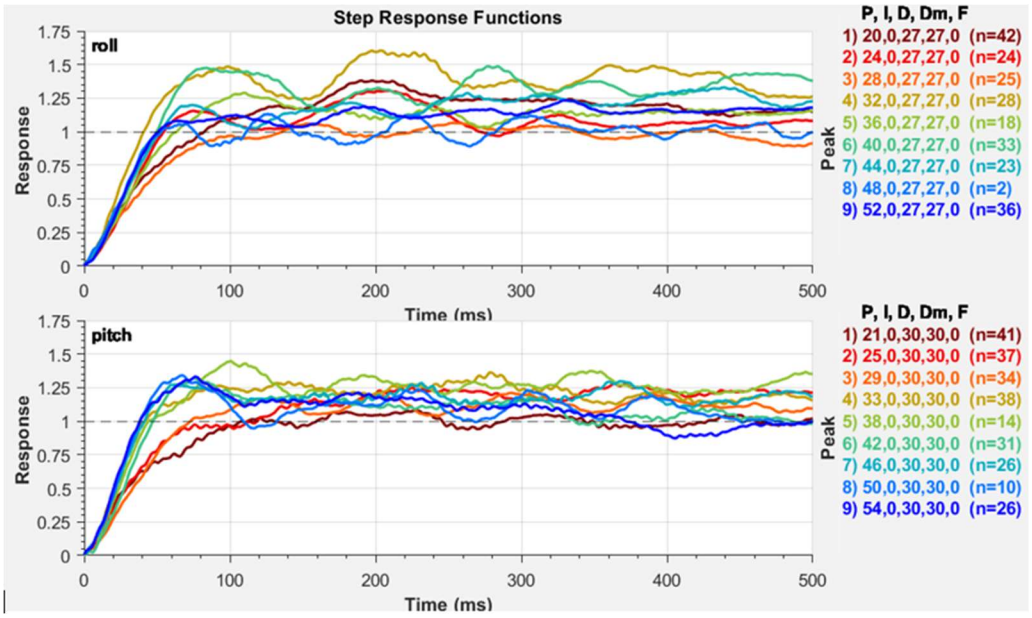

Figure 16 Dynamic Responses Corresponding to Slider Values

Among the responses, a value of 1.3 is chosen for its fast response and minimal oscillation for further tunning. However, a small steady-state error is observed in the roll response, and there is an overshot in the pitch response. To address these issues, the I-gain is increased for roll, and D-gain for pitch. The I-gain for Roll is adjusted by manipulating the "Drift-Wobble" slider, and the D-gain for Pitch is adjusted by manipulating the "Pitch damping" slider, using the same approach as adjusting the P&I slider.

Table 3 Sliders Values for Pitch Damping Test

Test Flight	Damping D Gain	Tracking P & I Gain	Stick Response	Dynamic Damping	Drift – Wobble	Pitch Damping	Pitch Tracking	Master Tracking
1	0.6	1	0	0	0	1	1	1
2	0.8	1	0	0	0	1	1	1
3	1.0	1	0	0	0	1	1	1
4	1.2	1	0	0	0	1	1	1
5	1.4	1	0	0	0	1	1	1
6	1.1	1	0	0	0	1	1	1

Table 4 Sliders Values for Multiplier Test

Test Flight	Damping D Gain	Tracking P & I Gain	Stick Response	Dynamic Damping	Drift – Wobble	Pitch Damping	Pitch Tracking	Master Tracking
1	1	1	0	0	0	1	1	0.60
2	1	1	0	0	0	1	1	0.75
3	1	1	0	0	0	1	1	0.90
4	1	1	0	0	0	1	1	1.05
5	1	1	0	0	0	1	1	1.20

Table 5 Sliders Values for I-gain Test

Test Flight	Damping D Gain	Tracking P & I Gain	Stick Response	Dynamic Damping	Drift – Wobble	Pitch Damping	Pitch Tracking	Master Tracking
1	1	1	0	0	0.25	1	1	0.9
2	1	1	0	0	0.5	1	1	0.9
3	1	1	0	0	0.75	1	1	0.9
4	1	1	0	0	1	1	1	0.9
5	1	1	0	0	1.25	1	1	0.9

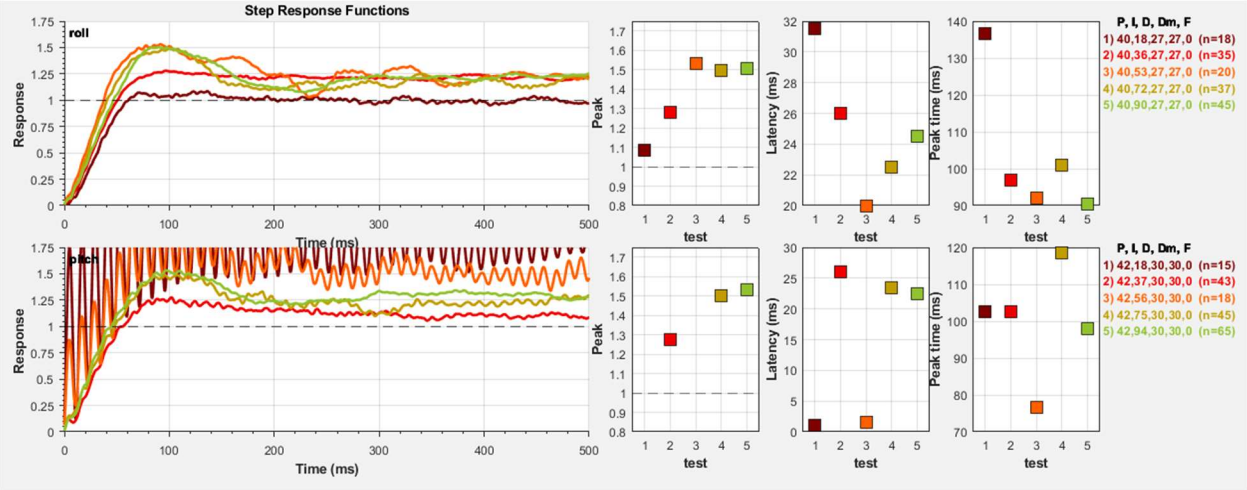

Figure 17 Dynamic Responses Corresponding to I-Slider Values

Decreasing the master multiplier reduces noise in the signal, resulting in less vibration. The vibration in the signal can be recognized by the drilling sound emitted by the motor when the drone is hovering.

After numerous flight tests, the optimal response is achieved with the following PID values for roll: P = 40, I = 18, D = 27; and for pitch, P = 50, D = 42. All the sliders are then adjusted to obtain the closest desired PID value for both pitch and roll.

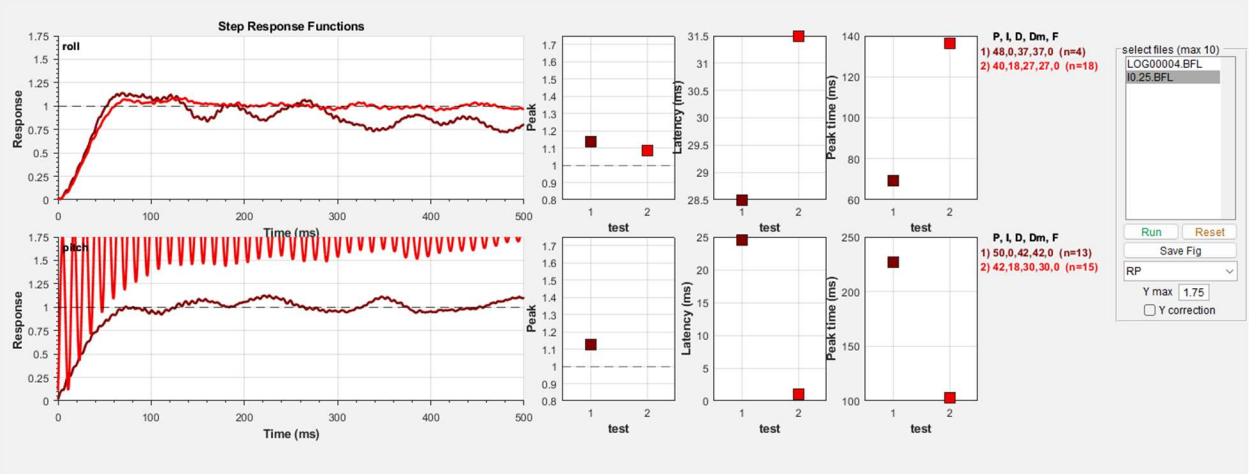

Figure 18 Current Response

Figure 19 Betaflight Sliders Values

7. Results

7.1. Vehicle Performance

With multiple flight tests, the drone consistently performed the way it was intended to. The flaps hinged inwards when the drone ascended and hinged outwards when descending. A consistent test was a huge success and a great accomplishment in the semester.

8. Summary

A successful working prototype has been produced that can take flight. Proportional Integral Derivative (PID) tuning has been accomplished to ensure a faster and more accurate response to the control system for this current model.

Figure 20 3D Printed Prototype

The 3D-printed drone achieved an experimental time of 3 seconds, which exceeded the calculated time of 2.52 seconds.

9. Conclusion

As the semester ended, some noticeable accomplishments included having a working prototype that, when dropped from 30ft, had a free fall time of 3 seconds. The steps to getting to having a working prototype took many iterations and design changes. Rather, there were issues with stability or vibrations. Each iteration made the structure more stable, prone to fewer vibrations, and a good learning experience. While a working prototype is a big accomplishment, there are numerous ways to improve the free fall time.

10.Future Work

Next semester's plan is to increase the drone's descent time for the next semester. To accomplish this goal, two approaches can be investigated: increasing the surface area of the flaps and reducing the weight. While increasing the surface area of the flaps will dramatically impact the time of descent, it may lead to a challenge when it comes to printing.

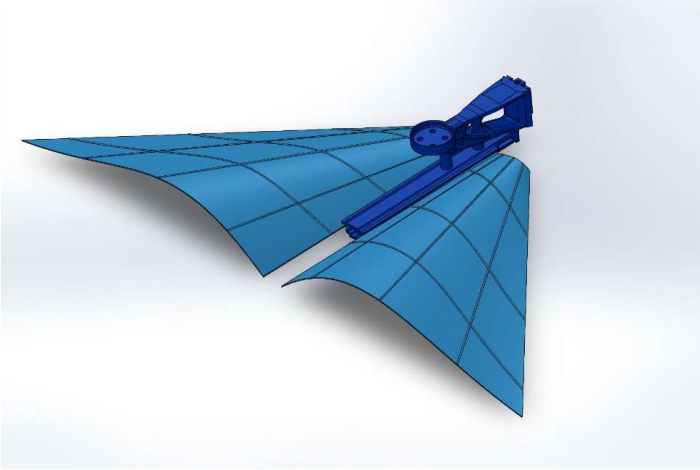

Figure 21 Current Design of the Flaps

Another note is that when the length of the flaps is increased, there is a constant breakage at the same spot. The future plans are to either increase the thickness of the flaps, create a thicker stiffener for the wings, or change the print orientation.

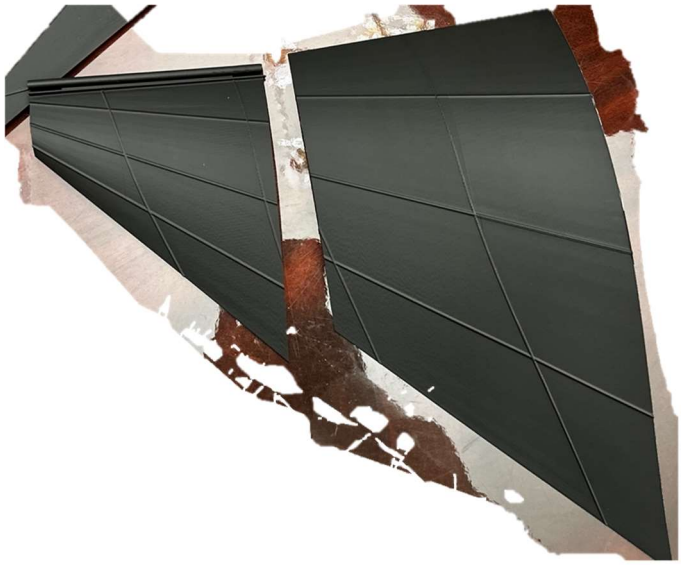

Figure 22 Breakage on Flaps

Reducing the weight of the overall drone will increase the time of descent. The infill density and pattern will be investigated without affecting the drone's performance. Also, the model should be looked at overall and investigated where any material can be removed without sacrificing structural integrity.

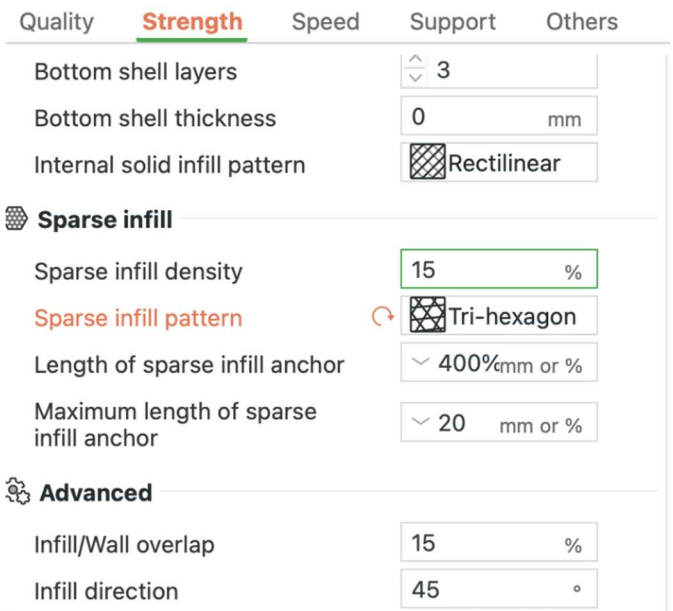

Figure 23 Changing Infill

Acknowledgments

Event Coordinator
Dr. Taylor
taylorrm@uta.edu

Event Sponsors

THE STEVEN C. & MARGARET S.
WHEELWRIGHT
FAMILY FOUNDATION

References

[1] 1Munson, B. R., Okiishi, T. H., Huebsch, W. W., and Rothmayer, A. P., Fundamentals of Fluid Mechanics, Hoboken, NJ: John Wiley et Sons, Inc., 2013.

[2] 1Goodno, B. J., and Gere, J. M., *Mechanics of Materials*, Boston, MA: Cengage Learning, 2018.

Appendix

1.1 Drone Arm 1 Analysis

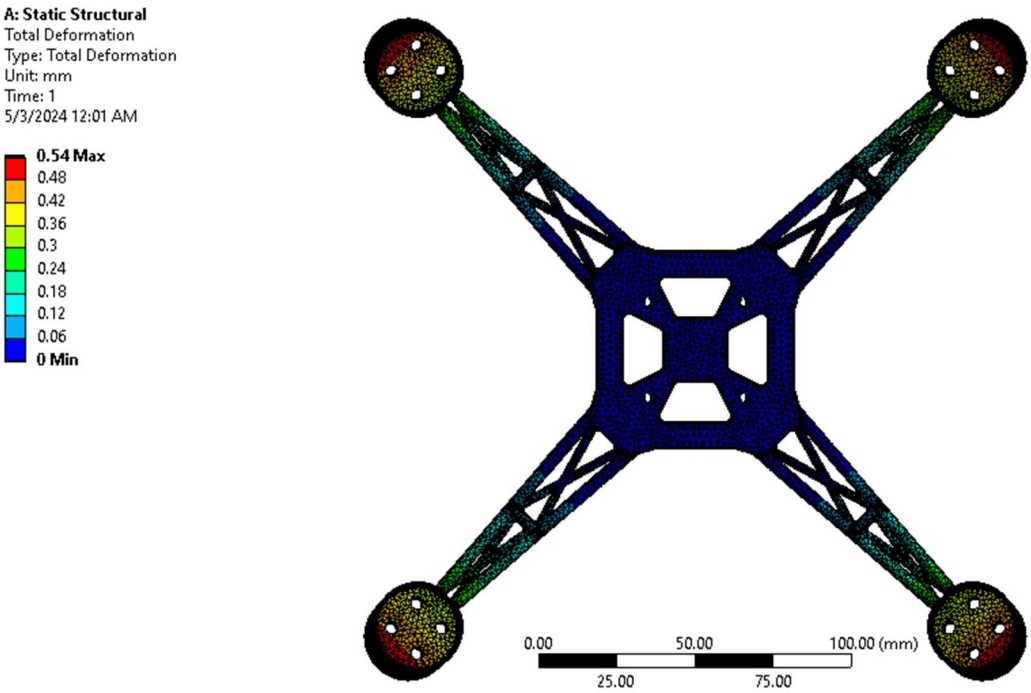

Figure 24 Total Deformation for Static Structural 1st Iteration Arm

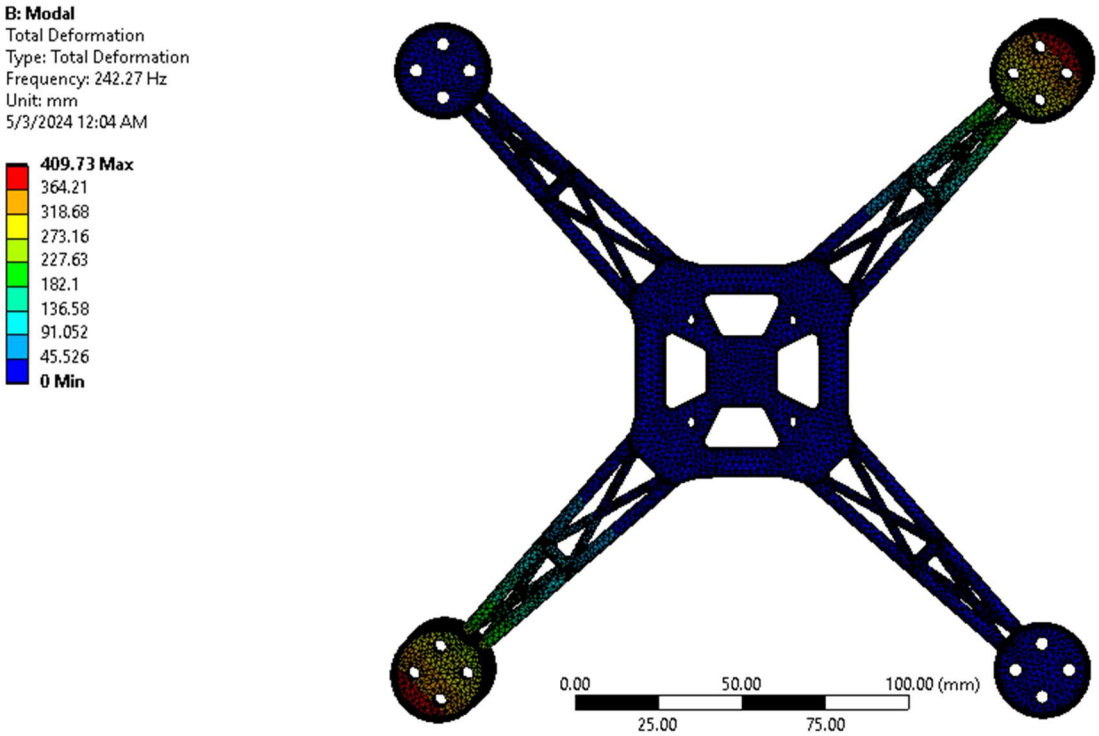

Figure 24 Total Deformation for Modal 1st Iteration Arn

1.2 Free Fall Analysis

Height	9.44 m	30 ft	Latitude	32.72956 N		0.57124		
			Longitude	-97.11452 E				
density of air	1.156 Kg/m^3	density at 90 F	Elevation	189.89 m				
drag coef	1.75							
g	9.7947 m/s^2							

Length(m)	Area	Terminal Velocity	Drag force	time for term	Distance travelled	Distance left after reaching terminal velocity	Time for fall after reaching terminal velocity	Total time for descent
0.3	0.09	6.45	3.79	0.66	2.12	7.32	1.13	1.79
0.4	0.16	5.11	4.22	0.52	1.33	8.11	1.59	2.11
0.5	0.25	4.35	4.77	0.44	0.96	8.48	1.95	2.39
0.6	0.36	3.87	5.45	0.40	0.76	8.68	2.24	2.64
0.7	0.49	3.55	6.26	0.36	0.64	8.80	2.48	2.84
0.8	0.64	3.33	7.18	0.34	0.57	8.87	2.66	3.00
0.9	0.81	3.17	8.23	0.32	0.51	8.93	2.82	3.14
1	1	3.05	9.40	0.31	0.47	8.97	2.94	3.25

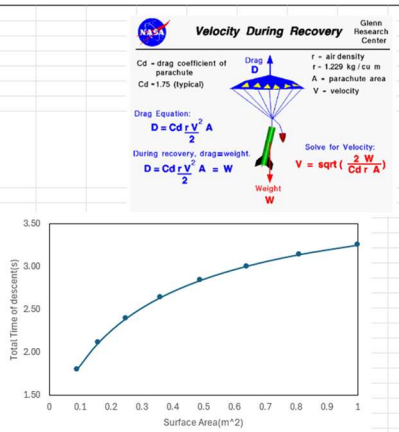

$$V_f = V_i + at$$

$$\Delta x = V_i t + \frac{1}{2} a t^2$$

$$V_f^2 = V_i^2 + 2a\Delta x$$

$$\Delta x = \frac{1}{2}(V_i + V_f)\, t$$

Figure 26 Free Fall Excel

1.3 Components Verification

MATLAB Code:

```
clc
clear all
```

```
format compact
format shortEng
% Given constants
mass = 0.68; % Mass in kg
g = 9.81; % Acceleration due to gravity in m/s^2
H_target = 9.144; % Target height in meters (30 ft)
time = 5; % Time to reach target height in seconds
V_battery = 22.2; % Battery voltage in Volts
I_battery = 1.2; % Assumed current draw in Amps
C=120; %discharge rate
I_battery_max = I_battery*C;
e_battery = 0.6; % Battery efficiency
e_Propeller = 0.8; % Propeller efficiency
rhoAir = 1.225; % Air density in kg/m^3
D_propeller = 0.155; % Diameter of propeller in meters (6.1 inches converted to
meters)
% Calculating required acceleration to reach target height
a = (2*H_target) / time^2; % Acceleration in m/s^2
aTotal = a + g; % Total acceleration including gravity
% Calculating required force
F_required = mass * aTotal; % Force required in Newtons

% Calculating thrust per motor
T_motorReq = F_required / 4; % Assuming 4 motors
% Motor RPM calculation
KV_motor = 1800; % Motor KV rating
RPM = KV_motor * V_battery; % No-load RPM
% Power calculation
P_electrical = V_battery * I_battery_max; % Electrical power in Watts
P_effective = P_electrical * e_battery;
T_motorProduce = (2 * rhoAir * pi * (D_propeller/2)^2 * P_effective^2)^(1/3) *
e_Propeller; % Thrust in Newtons
```